



POLITECNICO
MILANO 1863

DIPARTIMENTO DI MECCANICA



External Illumination Strategies for Melt Pool Geometry Monitoring in SLM

Mazzoleni, L.; Caprio, Leonardo; Pacher, M.; Demir, A. G.;
Previtali, B.

This is a post-peer-review, pre-copyedit version of an article published in JOM. The final authenticated version is available online at: <http://dx.doi.org/10.1007/s11837-018-3209-1>

This content is provided under [CC BY-NC-ND 4.0](https://creativecommons.org/licenses/by-nc-nd/4.0/) license



External Illumination Strategies for Melt Pool Geometry Monitoring in SLM

L. Mazzoleni*, L. Caprio, M. Pacher, A. G. Demir, and B. Previtali

Department of Mechanical Engineering, Politecnico di Milano, Via La Masa 1, 20156 Milan, Italy

*Corresponding author, luca.mazzoleni@polimi.it

Abstract

Coaxial monitoring in SLM can be applied using different configurations in terms of sensor choice and observed bandwidth. The use of external illumination to observe the melt pool geometry by suppressing the process emission is an option, where the melt pool geometry can be visualized independently from the changes in the emission behavior. However, the correct choice of the illuminator and the configuration in which it is implemented is an issue that requires further attention. This paper is aimed at obtaining a direct observation of the molten pool geometry using an external illumination source to suppress process emission. A coaxial imaging system was devised for this purpose and two different setups for light launching were designed and tested, namely a diode laser beam coaxial to the working laser and a lateral low-coherence laser illuminating the whole build platform. The advantages and criticalities of each experimental setup are extensively discussed. External illumination was found to be useful for interpreting directly the SLM melting conditions. Furthermore, the real scan position and velocity could be measured through an image processing algorithm on the captured frames.

Key words: selective laser melting, coaxial process monitoring, external illumination, melt pool observation

Introduction

Process observation plays a major role in promoting development of additive manufacturing technologies, especially Selective Laser Melting. The complex physical mechanisms involved in the melting process, with a wide range of non-equilibrium phenomena and over 50 variables influencing the on-going process [1], are not fully understood, and process observation is a valuable tool for enhancing the level of understanding and overcoming the empirical and iterative approaches commonly employed. Furthermore, in-line monitoring of the processing conditions could be highly beneficial for detecting process instabilities during the build. In fact, problems occurring while scanning could result in porosity formation [2], cracks [3] or even part failure [4]. The internal location of defects represents a prevalent issue for both post process inspection and repair, which often results impossible to obtain. As a consequence, detecting process anomalies during the on-going building is highly aspired, since it would enable an immediate in-situ correction otherwise unfeasible a posteriori. Several research efforts address the monitoring and quality assurance of SLM, with different sensors, setups and observed physical phenomena. Since laser processes are mostly thermal processes, NIR emission is captured to gather information on the molten pool emission shape [5],[6] or temperature [7] from a coaxial perspective. Alternatively, an off-axis configuration can be employed to look at the thermal behavior of the whole part, thus observing the lower heat conductivity associated with artificial flaws [8],[9]. Also, visible ranges are investigated to observe molten ejected particles [10]. While numerous process measurement modalities have been successfully demonstrated, the interpretation of the acquired signals still remains a challenging task. This may be attributed to the indirect signal acquisitions, such as process radiation, which can be hardly correlated to the actual physical phenomenon occurring in such a complex process. The difficulties in understanding data and the risk of false interpretation are especially evident when the employed sensor is spatially-integrated, since its one-dimensional output is not always easily linkable to the complex process physics. This research work is aimed at obtaining a direct observation of the melting conditions in order to have a more reliable and robust process evaluation. The molten pool geometrical properties could be a relevant

indicator for the on-going building, since the course of the melting process is strictly correlated to the final part quality in terms of density and geometrical precision [11]. Consequently, an external illumination light should be integrated in the monitoring module in order to dominate the strong emitted radiation associated with the interaction between laser and material, which would normally saturate a camera image. If the process emission contribution is lower than the external illuminator intensity, the camera sensor sees only the reflected light and consequently the surface conditions in correspondence of the processed zone are revealed [12], [13]. A coaxial imaging setup is presented, and two different implementations for the external illuminator are discussed, namely a coaxial and a lateral illumination setup. Once the external light source is integrated and its parameters tuned, the molten pool geometry can be directly visualized. Furthermore, process parameters can be measured from the acquired frames, such as the actual scan position and velocity.

An open SLM platform with monitoring module

A. Selective Laser Melting system

A SLM machine prototype namely Powderful was used in this work [4]. It features all the characteristics of a real industrial SLM machine, but it is suitable for research purposes thanks to its compact size (available workspace area of 60x60x20 mm³), reduced processable powder quantities (< 0.5 kg) and the possibility to fully customize the SLM system and the laser optical chain. The laser source employed in the experimentation was a single mode fiber laser with 250 W maximum power output (IPG YLR-150/750-QCW-AC, Cambridge, MA, USA). The laser optical chain was composed by a collimating unit, a two-lens system for setting the focal plane position (VarioScan 20, Scanlab, Puchheim, Germany) and a 420 mm f-theta lens. The main characteristics of the SLM system are summarized in Table 1.

Table 1. Open SLM platform Powderful main characteristics.

| Parameter | Value |
|--------------------------------------|--------------------------|
| Build platform area (DxWxH) | 60x60x20 mm ³ |
| Laser emission wavelength, λ | 1070 nm |
| Beam waist diameter d_0 | 70 μ m |
| Maximum laser power, P_{max} | 250 W |

B. Monitoring module

A coaxial monitoring module was chosen for the application, taking the advantage of a compact and less invasive design and the possibility to always image the working point of the laser independently of the beam movement. Accordingly, this setup eliminates the necessity to look simultaneously at the whole build platform and the area imaged by the sensor, i.e. the field of view, can be restricted to the dimensions of the processed zone, thus significantly reducing the data rate generated and enabling long term acquisitions [14]. The imaging optical chain and the sensor were jointed directly onto the machine working head via dichroic mirror, which allowed for splitting laser radiation and process light coming from the working platform. As depicted in the schematic representations of Figure 1, process light was transmitted through the f-theta lens and reflected by the two galvanometric mirrors. The dichroic mirror allowed for deflecting the observation wavelength towards the camera sensor, without influencing the processing laser path. In order to correctly set the imaging focal plane position onto the build platform and fix the desired magnification about 0.34, thus avoiding excessive spatial resolution and consequently data burden, a 120 mm objective lens was integrated just after the dichroic mirror. A short pass filter at 1000 nm was used to avoid possible laser back reflections damaging the imaging optical components (FSH1000, Thorlabs, Newton, NJ, USA). Other optical filters could be placed just before the camera sensor in order to observe predefined wavelength bands. The camera sensor chosen for the application was Ximea xiQ CMOS camera (Ximea xiQ USB Vision, Münster, Germany), a compact and high performance industrial camera which allows frame rates within the kHz range at a reduced pixel number. It features a pixel

size of $4.8 \times 4.8 \mu\text{m}^2$, thus obtaining a final spatial resolution of about $14 \mu\text{m}/\text{pixel}$. The set active pixel area was 304×304 pixels, ensuring a $4.3 \times 4.3 \text{ mm}^2$ field of view and an acquisition rate of 1200 Hz.

C. External illumination sources

An external illumination source for laser process observation should fulfil different requirements. The beam intensity per unit area should be enough to dominate the emitted radiation. For such purpose, a monochromatic external light is preferable, since an adequate optical filter centered on the external illumination wavelength and placed before the camera sensor could be highly beneficial for transmitting the external reflected light and eliminating the broadband radiation emitted from the processed zone. Furthermore, the illumination properties should not lower the information content of the image. In this context, speckle formation could represent an important issue. Speckles refer to non-uniform illumination intensity encountered with coherent light sources, which is caused by the constructive and destructive interference of the illuminating light when interacting with a rough surface. Finally, the configuration in which the illuminator is implemented has a relevant impact on the final illumination system characteristics. A coaxial implementation of the light source implies a less invasive solution and the need for a lower power light source. In fact, in a coaxial system, the illuminated area moves together with the processed zone. Consequently, the external light can be focused just on the molten pool region, allowing for high intensity per area levels. The second possible setup is a lateral light source illuminating the whole build platform. Diffuse light sources such as LED are often employed in imaging applications due to their excellent illumination properties. Nevertheless, the application for laser processes observation could result critical, since the high-divergence nature of these light sources may provide insufficient beam intensity per unit area to dominate the strong radiation emitted by the process. As a consequence, high power light sources are needed to correctly illuminate the process area.

Based on the aforementioned considerations, the diode laser Z-Laser ZQ1 (Z-Laser ZQ1, Freiburg, Germany) was selected for a coaxial implementation. Diode lasers, thanks to their high power and low-divergence nature, allow for higher beam intensity per unit area than comparable diffuse lights, thus being suitable for dominating process emission in a coaxial implementation [15]. Nevertheless, their coherent nature may represent a problem as regards speckle formation. A 670 nm wavelength was chosen considering the optical chain transmission constraints, especially the pre-existing galvanometric mirrors that attenuated almost 80% intensity of the incoming radiation between 750 nm and 1000 nm, thus consistently limiting the external light reaching the build platform in a coaxial implementation. Its maximum power was 0.4 W, and a manual focus allows for adjusting the rectangular spot dimensions. On the other hand, the illuminator chosen for illuminating laterally across the entire build platform was Cavitar Cavilux HF (Cavitar, Cavilux HF, Tampere, Finland). It consisted of a powerful pulsed diode laser light source, with pulse peak power equal to 280 W. The light source featured a low degree of coherence, thus assuring a uniform illumination without speckle formation. After a fiber optic light guide with a core diameter of 1.5 mm, a focusing optics allowed for adjusting the illumination spot size. The high power and the large spot, with diameter in the range of some centimeters, made this light source suitable for a lateral illumination, while problematic for a coaxial implementation due to the excessive beam size for the existing optical components and the powerful internal reflections saturating the camera sensor. The chosen illuminators for the two configurations and their main characteristics are summarized in Table 2.

Table 2. Overview of the experimental configurations and external light sources chosen for the work.

| Configuration | Coaxial | Lateral |
|---------------------------------------|--------------|--------------------|
| Laser model | Z-Laser ZQ1 | Cavitar Cavilux HF |
| Wavelength [nm] | 670 ± 10 | 640 ± 10 |
| Max. peak power [W] | 0.4 | 280 |
| Max. duty cycle [%] | 100 | 2 |
| Max. pulse duration [μs] | ∞ | 10 |

D. Definition of the performance criteria

The beam intensity on the powder bed is a good indicator of the illumination capacity for laser processes visualization, which is calculated as:

$$I = \frac{P_{peak} \cdot T}{A_{beam}} \quad (1)$$

where T is the total transmissivity of the optical path and A_{beam} is the projected beam area on the powder bed surface. The intensities were calculated as a function of the beam optical path transmittance and size for both setups. A low beam intensity value may represent a problem for dominating the radiation emitted from the process, resulting in a disturbed visualization of the processed zone.

The illumination uniformity level and the speckle influence were quantified through the speckle contrast coefficient. Speckle contrast C is defined as the ratio of the standard deviation of the intensity fluctuation to the mean intensity [16]:

$$C = \frac{\sigma_I}{\mu_I} \quad (2)$$

The higher the magnitude of speckle contrast, the higher the speckle disturbances on surface visualization. Furthermore, the total number of saturated pixels reducing the image information content was evaluated for both illumination systems.

Finally, motion blur was taken into account in order to achieve high quality images. Motion blur refers to a decrease of image sharpness when the sensor is exposed to a moving object. In general terms, the higher the exposure time, the lower the image sharpness, according to the following relation:

$$B = \frac{v_{object} \cdot t_{exposure}}{r_s} \quad (3)$$

where B is the magnitude of blur in pixels, v_{object} is the velocity of the imaged object, in this case equal to the scan velocity employed, $t_{exposure}$ is the exposure time of the camera and r_s is the spatial resolution of the monitoring system. In most cases, blurring becomes an issue when it exceeds one pixel. When using a powerful external light source, the camera sensor is excited only by the external reflected light independently of sensor exposure time. Consequently, the motion blur depends on the temporal duration of the light pulse t_{on} as follows:

$$B = \frac{v_{object} \cdot t_{on}}{r_s} \quad (4)$$

Implementation of different illuminators

A. Coaxial illumination setup

The coaxial implementation of the diode laser took place in a beamsplitter, which was added just before the objective lens module. A beam splitter was chosen since it allowed reflecting the external light downwards to illuminate the process area, but at the same time it transmitted the reflected light coming from the process area towards the camera sensor, as depicted in Figure 1. The integration of the diode laser in the pre-existing laser optical chain implies several criticalities. First, since laser optical elements are not optimized for external illumination wavelength, unwanted back reflections inside the optical chain might saturate camera sensor, thus hiding the build platform visualization. In the application under analysis, the most critical optical component was the f-theta lens. At 670 nm, 70% of the incoming radiation was transmitted towards the build platform, while the 30% was reflected directly to the camera sensor. A stationary saturated square appeared on the camera sensor, as the one reported in Figure 2a. In order to eliminate this unwanted direct reflection, the diaphragm

revealed to be a powerful tool. The closure of the iris diaphragm aperture acted as a spatial filter, thus reducing the amount of direct reflected light onto the sensor, without affecting the image formation onto the sensor. By closing the diaphragm aperture (f-number about 8 or higher), the direct back reflection was completely suppressed, as shown in Figure 2. Another important noise source was represented by the broadband process emission. The usage of a bandpass filter around the illumination wavelength just before the sensor allowed reducing the emission contribution captured by the camera sensor. Finally, a perfect alignment of the laser source was needed in order to center the illumination diode laser area with the processing laser. An optomechanical mount for precision position adjustment was used and a square illumination area of about 5 x 5 mm² was obtained via manual focus adjustment of the diode laser ZQ1. From the full sensor image of Figure 2b, it can be noticed that the coaxial illumination beam successfully illuminated the area of interest, highlighted by dashed lines (304 x 304 pixels, corresponding to a 4.3 x 4.3 mm² FOV).

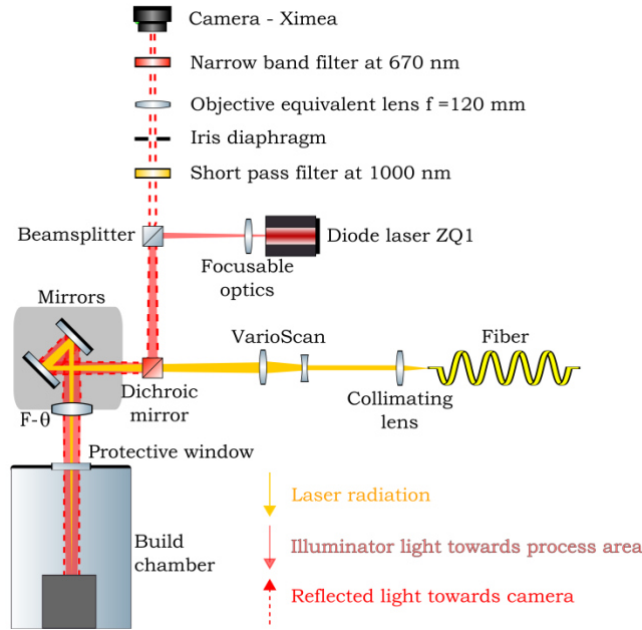


Figure 1. Schematic representation of the coaxial illumination system.

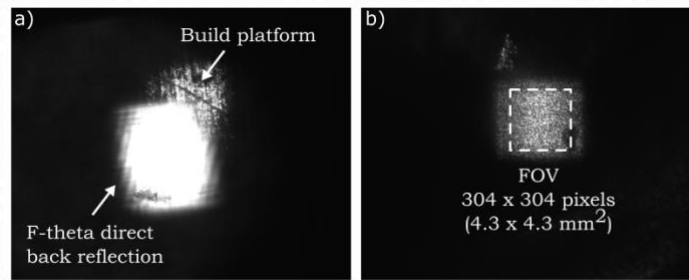


Figure 2. Full sensor (1280 x 1024 pixels) acquired frames: a) f-theta back reflection saturating the camera sensor, b) final configuration, with the illuminator spot size restricted to the designed field of view.

B. Lateral illumination setup

The lateral implementation of the low-coherence light source revealed to be less critical than the coaxial integration of the external light beam. The pre-existent laser optical chain did not represent an issue for light launching, since the only optical element between the external light source and the build platform was the protective window of the chamber (Figure 3). Furthermore, the pre-existent laser optical chain equally attenuated both process emission and reflected external light, so no issues were associated with laser optical chain back reflections or damping effect. Since illumination beam did not follow process laser movements, the only precaution was to illuminate the whole build platform, around 50x50 mm² without exceeding in spot dimension

in order to have sufficient beam intensity on the powder bed to dominate process emission. Again, a narrowband pass filter was inserted before the camera sensor to reduce the broadband process emission.

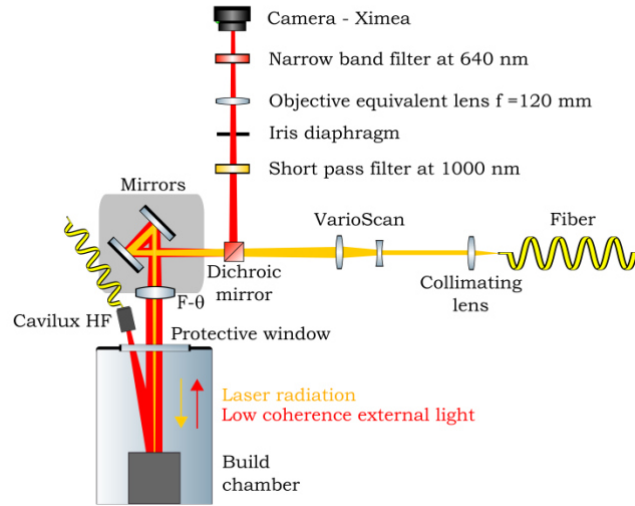


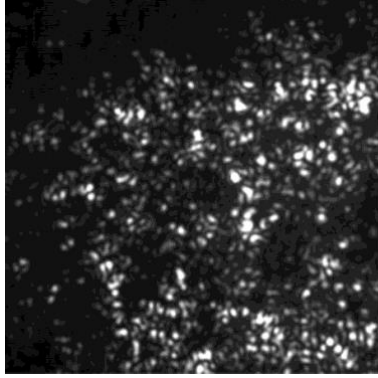
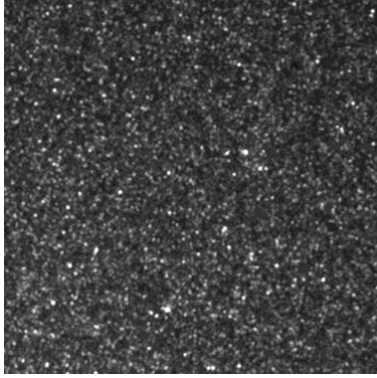
Figure 3. Schematic representation of the lateral illumination system.

Analysis of the illuminated monitoring system

A. Evaluation of image properties

Illumination played a large role in achieving high quality images, thus useful for qualitative and quantitative extraction of relevant process features. The illumination properties of the two different light sources were evaluated when illuminating the SLM powder bed, without laser processing. The two images in Table 3 show a 50 μm thick powder bed of AISI 316L stainless steel powder (powder size distribution D10: 23 μm , D50: 32 μm , D90: 44 μm) acquired through the two illumination systems. When illuminating the powder by means of the coaxial laser diode, the surface shows a multitude of bright spots, which lead to saturated pixels and dark spots. Due to the coherent nature of the coaxial diode laser, the scattered light has components with different delays, which are caused by the roughness of the illuminated surface. As the scattered light propagates further, these coherent but dephased components interfere and produce granular intensity pattern called speckle. The pattern, as the one in Table 3, consists of bright spots created by constructive interference, dark spots created by destructive interference, and areas with intermediate brightness levels. The speckle contrast parameter was evaluated for both the illumination systems. All the results are reported in Table 3. From the analysis, the low-coherence light reveals to be more suitable for powder bed visualization. The coaxial diode laser Z-Laser ZQ1 suffers from speckle formation, highlighted by a speckle contrast that is approximately double than the Cavitar Cavilux HF laser source, thus making powder visualization a challenging task. The bright spots induced by positive light interference lead also to a significantly higher number of saturated pixels, thus reducing the information content of the image.

Table 3. Powder bed visualization with the two illumination systems.

| | Coaxial diode laser | Lateral low-coherence diode laser |
|---|---|--|
| Powder bed, 304 x 304 pixels, FOV 4.3 x 4.3 mm ² |  |  |
| Speckle contrast | 0.84 | 0.38 |
| Saturated pixels / # | 377 | 44 |

A preliminary experimental campaign was performed to test the capability of the two illumination systems to visualize the melt pool geometry when processing the powder bed. An AISI 316L cube (5x5x5 mm³) was built and monitored by using the two different illumination systems. The laser power was set at 200 W, the scan velocity at 400 m/s. The hatch distance and the layer thickness were 70 μ m and 50 μ m respectively. The active area of the camera sensor was reduced at 304x304 pixels, with an acquisition frequency of 1200 Hz. Camera exposure time was set to its minimum, equal to 29 μ s, in order to reduce process emission contribution as much as possible. In fact, Cavitar Cavilux HF light source allows for maximum laser pulse duration equal to 10 μ s, and time intervals outside the 10 μ s light pulse only increase the amount of process emission caught by the sensor, as depicted in Figure 4, thus making surface visualization more difficult. Furthermore, enlarging the exposure time implies a lower capability of detecting dynamic events that could be of interest for the on-going process, since the camera sensor integrates all the light contributions that reach the sensor within exposure time, and fast dynamic events could be lost.

Once camera parameters have been set, illumination should be tuned. For Z-Laser ZQ1 diode laser, a pulse duration equal to 29 μ s and the maximum power were set. This allowed for the maximum possible diode laser light contribution against process emission. For the same reason, a pulse duration of 10 μ s with a peak power of 280 W was fixed for Cavitar Cavilux HF. According to Eq. 4, the magnitude of motion blur associated with the two systems was about 0.8 and 0.3 respectively, thus ensuring high sharpness images. The camera acquisition and the external illumination pulses were synchronized by means of an external TTL signal in order to have the same illumination conditions among frames. A temporal delay t_{delay} equal to 1 μ s between the rising edge of the TTL signal and the start of the pulse was set for Cavitar Cavilux HF to avoid possible light losses caused by intrinsic limitations on the synchronization of the camera and external illuminator. All parameters and results are summarized in Table 4. A visual representation of the chosen configuration for the camera and the illuminators is depicted in Figure 4.

Table 4. Summary of process, camera and illuminator parameters.

| Process parameter |
|-------------------|
|-------------------|

| | | |
|---------------------------------|------------------------|------------------------|
| Material | AISI 316L | |
| Power | 200 W | |
| Scan speed | 400 mm/s | |
| Hatch distance | 70 μm | |
| Layer thickness | 50 μm | |
| Camera parameter | | |
| ROI | 304 x 304 pixels | |
| Frame rate | 1200 fps | |
| Exposure time | 29 μs | |
| Illuminator parameter | Coaxial | Lateral |
| Laser source | Z-Laser ZQ1 | Cavitar Cavilux HF |
| Power | 0.4 W | 280 W |
| PRR | 1200 Hz | 1200 Hz |
| Pulse duration | 29 μs | 10 μs |
| Duty cycle | 3.5 % | 1.2 % |
| Estimated optical transmittance | 15% | 85% |
| Beam intensity on powder bed | 0.23 W/cm ² | 14.9 W/cm ² |

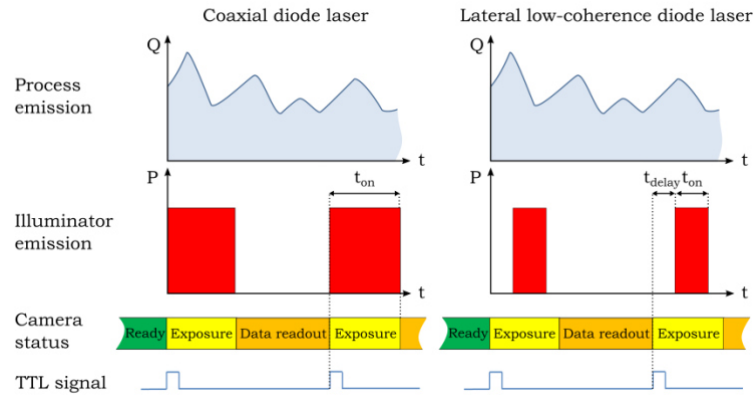


Figure 4. Schematic visualization of the camera and illumination parameters chosen for the two illumination systems.

Figure 5 reports an example of the acquired images for each illumination system. The coaxial diode laser illumination system reveals to be problematic for proper melt pool visualization. Two main problems are associated with this type of illuminator. First, the low illumination quality leads to the formation of speckle pattern, especially in the solidified material, which is highly reflective. The bright spots tend to saturate the camera sensor, thus hiding the melt pool contours. The melt pool appearance, characterized by a dark aspect and dynamic bright oscillations of the liquid pool, results displayed to be confused with the bright and dark spots generated by the coherent light source. Secondly, the beam intensity reveals to be insufficient for dominating process emission. In fact, bright ejections of molten particles are clearly visible while processing the powder bed. The camera sensor sees these high temperature particles as bright spots, since emitted light intensity is comparable with the external illumination amount. The insufficient incident light on the processing zone may be attributed both to the relatively low laser source power, 0.4 W, and the several light attenuations during the coaxial light launching due to the existing laser optical components, optimized for 1070 nm wavelength. The estimated optical transmittance is 15%, thus resulting in a beam intensity on the powder bed two orders of magnitude lower than the one reached with the lateral low-coherence laser, as reported in Table 4. The difficulties in detecting the molten boundaries are especially evident when extracting the image gray levels in correspondence of a straight line centered on the molten pool (blue dotted line of Figure 5). From the gray levels distribution, only the bright spot associated with the direct interaction between the laser and the powder is detectable, while no melt pool tail can be extracted.

Lateral Cavitax Cavilux HF illumination reveals to be more suitable for melt pool observation. The uniform powerful light allows for sight of the powder bed, the molten material and the solidified material, as depicted in Figure 5. Again, strong uniform reflections from the already solidified material are present, due to the reflecting nature of the surface of solidified AISI 316L and the almost perpendicular position of the illuminator with respect to the processing zone. These strong reflections can occasionally disturb a clear observation of the molten region. Nevertheless, the molten pool is identified due to its dark appearance. The beam intensity on the powder bed results to be sufficient for eliminating process emission influence. In fact, even if a bright spot always appears where the direct interaction between the laser source and the material takes place, the dark melt pool tail and the molten zone shape are detectable. By extracting the gray levels on a straight line in correspondence of the molten zone, the lower gray values are associated with the molten region due to the increased absorptivity of the liquid phase. An intensity peak is reached in correspondence of the zone of direct interaction between the laser and the powder due to the powerful process emission. On the contrary, the reflecting behavior of the solidified material results in higher recorded intensities, up to saturation, while a more irregular gray level pattern is associated with the powder grains distribution. Although the intrinsic difficulties in image processing, the acquired frames are rich in information and a further investigation should focus on the extraction and analysis of process features by means of ad-hoc image processing algorithms.

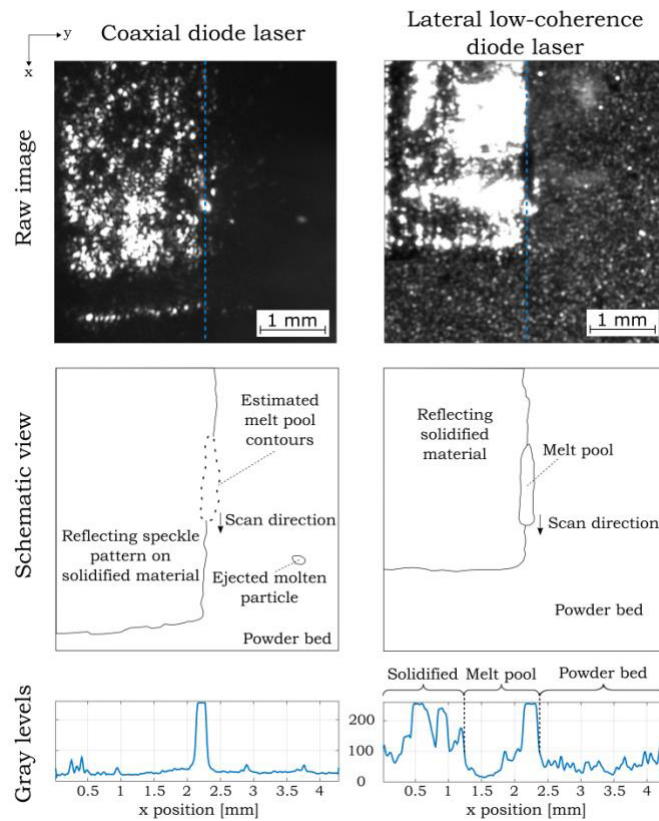


Figure 5. Melt pool images acquired with the two illumination systems. From the top: raw image, explicative representation and gray levels in correspondence of the blue dotted line.

B. Measurement of position and scan speed

External illumination enables not only a direct visualization of the molten pool, but also the monitoring of process parameters such as the scan position and speed. The low-coherence diode laser in a lateral configuration was chosen for the purpose, due to its higher illumination properties. Since the observed powder bed is stationary and the area imaged by the sensor in a coaxial setup is moving together with the processing laser beam, a relative displacement can be calculated between two consecutive frames. The measurement procedure is based on cross correlation algorithm. A reference subset in frame i should be fixed on the stationary powder bed far away from the processing zone, thus avoiding process disturbances, and at a distance from the image edges compatible with the maximum possible feed and including an additional safety zone. The

new position of the reference subset in the following frame $i + 1$ can be identified by finding the maximum normalized cross correlation of the reference subset in the consecutive image. The normalized cross-correlation (NCC) is defined as [17]:

$$\gamma(u, v) = \frac{\sum_{x,y} [f(x,y) - \bar{f}_{u,v}] [t(x-u, y-v) - \bar{t}]}{\{\sum_{x,y} [f(x,y) - \bar{f}_{u,v}]^2 \sum_{x,y} [t(x-u, y-v) - \bar{t}]^2\}^{0.5}} \quad (5)$$

where f is the image, t is a $m \times n$ subset, \bar{t} is the mean of the subset, $\bar{f}_{u,v}$ is the mean of $f(x, y)$ in the region under the subset and $\gamma(u, v)$ is the normalized cross-correlation coefficient as a function of the horizontal and vertical displacements u and v of the searched subset t . The maximum value of $\gamma(u, v)$ is reached when subset t in frame i and the corresponding region in frame $i + 1$ are matched. An example of displacement reconstruction is illustrated in Figure 6. By iteratively employing the aforementioned procedure on consecutive frames, a position map for each layer can be reconstructed, as reported in Figure 7a. Furthermore, from NCC relative displacement reconstruction, the actual scan speed can be measured and compared with the nominal value, i.e. 400 mm/s for the application under analysis. The actual scan velocity is simply evaluated as the displacement between two consecutive frames multiplied by the camera frame rate. Figure 7b shows an example of the calculated results. The regime scan speed matches the nominal scan speed, but transient acceleration and deceleration periods at the beginning and end respectively of every scan line can be noticed. In common practice, few of the key input process parameters are monitored. Measuring both process signals and input parameters could be an effective way to have a complete picture of the on-going processing conditions, thus understanding if the possible process anomalies are correlated to process parameters variations or unpredicted events. The dynamic behavior of the galvanometric mirrors, with a decrease of scan velocity in correspondence of the reorientation of the scan direction up to 100 mm/s, could have a relevant impact on the processing conditions that is not imputable to accidental instabilities, but a corrective action, such as sky writing or adaptation of laser power, should be undertaken.

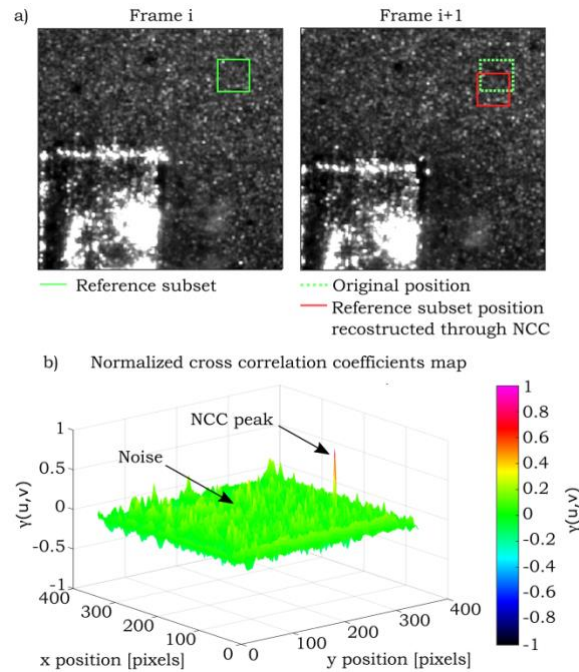


Figure 6. a) Measurement of the relative displacement between two consecutive frames by finding the maximum NCC, b) example of NCC correlation coefficient map on frame i+1. A distinct peak value is found when the reference subset of frame i matches its corresponding position in frame i+1.

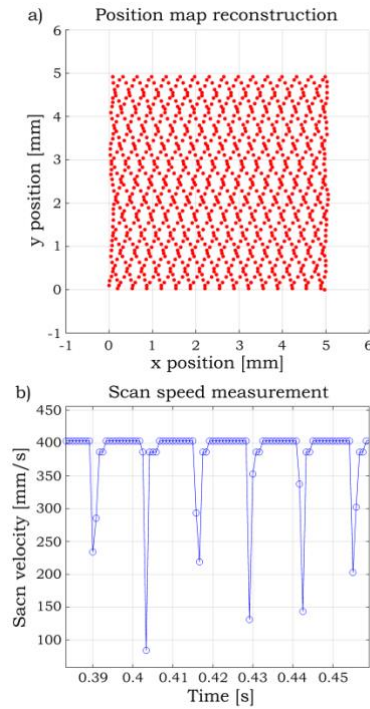


Figure 7. a) Final spatial map obtained by applying NCC algorithm on a frame sequence and b) actual scan speed calculated through NCC algorithm.

Conclusions

In this work, the use of external illumination in combination with a coaxial monitoring module for melt pool observation is investigated. Two external illumination systems are tested: the first setup uses a diode laser coaxially integrated in the laser optical chain, while the second one employs a low-coherence monochromatic light in a lateral configuration. The choice of the illumination system reveals to be a key factor for a successful observation of the processed surface due to different illumination properties of the implemented light sources. In particular, the coaxial diode laser suffers from speckle formation, which lowers the information content of the acquired frames, thus preventing a clear observation of the processed zone. Nevertheless, a coaxial implementation of the illuminator could assure several advantages, namely no limitations regarding the movement of the laser head, a compact and less invasive design and the need for a lower power diode laser source, due to the possibility to focus the entire illuminating beam on the processed area. Consequently, its implementation should be further investigated in a tailored optical chain, thus avoiding light losses and internal back reflections. On the other hand, the lateral low-coherence light succeeds in illuminating uniformly the build platform and visualizing the processed zone. The employment of an external illuminator reveals to be a powerful tool for revealing the real melting conditions, usually masked by the strong process emission, thus enabling a direct observation of the complex SLM physics. Furthermore, the visualization of the processed surface allows for measuring the actual scan position and velocity, which could lead to a deeper understanding of the real state of the process.

Acknowledgements

This work was supported by European Union, Repubblica Italiana, Regione Lombardia and FESR for the project MADE4LO under the call "POR FESR 2014-2020 ASSE I - AZIONE I.1.B.1.3". The authors gratefully acknowledge Adige of BLM Group for their technical support and equipment funded with the contribution of the Autonomous Province of Trento, Italy, through the Regional Law 6/98 in the granted Project: LT4.0. The authors would like to acknowledge Z-Laser for the technical support and hardware for external illumination. The authors gratefully acknowledge IPG Photonics Italy and Renishaw for their collaboration.

References

- [1] T. G. Spears and S. A. Gold, "In-process sensing in selective laser melting (SLM) additive manufacturing," *Integr. Mater. Manuf. Innov.*, 2016.
- [2] H. Gong, K. Rafi, H. Gu, T. Starr, and B. Stucker, "Analysis of defect generation in Ti – 6Al – 4V parts made using powder bed fusion additive manufacturing processes &," *Addit. Manuf.*, vol. 1–4, pp. 87–98, 2014.
- [3] K. Kempen, B. Vrancken, S. Buls, L. Thijs, J. Van Humbeeck, and J.-P. Kruth, "Selective Laser Melting of Crack-Free High Density M2 High Speed Steel Parts by Baseplate Preheating," *J. Manuf. Sci. Eng.*, vol. 136, no. 6, p. 61026, 2014.
- [4] A. G. Demir, L. Monguzzi, and B. Previtali, "Selective laser melting of pure Zn with high density for biodegradable implant manufacturing," *Addit. Manuf.*, vol. 15, pp. 20–28, 2017.
- [5] S. Clijsters, T. Craeghs, S. Buls, K. Kempen, and J. P. Kruth, "In situ quality control of the selective laser melting process using a high-speed, real-time melt pool monitoring system," *Int. J. Adv. Manuf. Technol.*, vol. 75, no. 5–8, pp. 1089–1101, 2014.
- [6] U. Thombansen and P. Abels, "Observation of melting conditions in selective laser melting of metals (SLM)," vol. 9741, p. 97410S, 2016.
- [7] Y. Chivel and I. Smurov, "On-line temperature monitoring in selective laser sintering/melting," *Phys. Procedia*, vol. 5, no. PART 2, pp. 515–521, 2010.
- [8] H. Krauss, T. Zeugner, and M. F. Zach, "Thermographic process monitoring in powderbed based additive manufacturing," vol. 177, pp. 177–183, 2015.
- [9] H. Krauss, C. Eschey, and M. F. Zach, "Thermography for Monitoring the Selective Laser Melting Process," pp. 999–1014, 2012.
- [10] B. Lane, E. Whitenton, and S. Moylan, "Multiple sensor detection of process phenomena in laser powder bed fusion," vol. 9861, p. 986104, 2016.
- [11] A. G. Demir, P. Colombo, and B. Previtali, "From pulsed to continuous wave emission in SLM with contemporary fiber laser sources: effect of temporal and spatial pulse overlap in part quality," *Int. J. Adv. Manuf. Technol.*, vol. 91, no. 5–8, pp. 2701–2714, 2017.
- [12] B. Regaard, S. Kaierle, W. Schulz, and A. Moalem, "Advantages of coaxial illumination for monitoring and control of laser material processing," *Proc. ICALEO*, pp. 915–919, 2005.
- [13] L. Caprio, A. G. Demir, and B. Previtali, "Comparative study between CW and PW emissions in selective laser melting," *36th Int. Congr. Appl. Lasers Electro-Optics ICALEO*, vol. 32305, p. 1304, 2017.
- [14] S. Berumen, F. Bechmann, S. Lindner, J. P. Kruth, and T. Craeghs, "Quality control of laser- and powder bed-based Additive Manufacturing (AM) technologies," *Phys. Procedia*, vol. 5, no. PART 2, pp. 617–622, 2010.
- [15] U. Thombansen and M. Ungers, "Illumination for process observation in laser material processing," *Phys. Procedia*, vol. 56, no. C, pp. 1286–1296, 2014.
- [16] J. W. Goodman, "Some fundamental properties of speckle," *J. Opt. Soc. Am.*, vol. 66, no. 11, p. 1145, 1976.
- [17] J. P. Lewis, "Fast Normalized Cross-Correlation," *Vis. Interface*, vol. 1995, no. 1, pp. 1–7, 1995.